First-principles study of the electronic stopping power of indium for protons and He ions

Shi-Ming Li,[1] Fei Mao [ORCID],[1,*] Xu-Dong Zhao,[1] Bing-Sheng Li,[2] Wen-Qi Jin [ORCID],[1] Wen-Qi Zuo,[1]
Feng Wang [ORCID],[3] and Feng-Shou Zhang [ORCID][4]

[1]*School of Nuclear Science and Technology, University of South China, Hengyang 421001, China*
[2]*State Key Laboratory for Environment-friendly Energy Materials, Southwest University of Science and Technology,
Mianyang, Sichuan 621010, China*
[3]*School of Physics, Beijing Institute of Technology, Beijing 100081, China*
[4]*The Key Laboratory of Beam Technology of Ministry of Education, College of Nuclear Science and Technology,
Beijing Normal University, Beijing 100875, China*

The electronic stopping power of protons and He ions traveling along the channeling and off-channeling trajectories in indium is reported based on time-dependent density functional theory combined with Ehrenfest molecular dynamics simulations. We provided an intuitive description of the electronic stopping power for a wide range of ion energies, and revealed the microcosmic excitation mechanism of the semicore $4d$ electrons of In. The velocity-proportional electronic stopping power and the kink velocity which is due to $4d$-electron excitation are reproduced in the low-energy regime. Because the $5s5p$ valence electrons are uniformly distributed in indium, the electronic excitation of valence electrons via Coulomb scattering is independent of the impact parameter in the investigated velocity range. On the contrary, due to the highly localized nature of semicore electrons, the excitation of $4d$ electrons increases significantly with decreasing of the impact parameter, which suggests that it is triggered by direct ion-electron collision. Our calculated stopping power is in quantitative agreement with the experimental data up to the stopping maximum, and showed that the stopping power obtained from the off-channeling geometry is greatly improved in comparison with the channeling results. Finally, we examined the extent to which the linear response theory is applicable to describe the electronic stopping power by quantifying the velocity dependence of the mean steady-state charge of protons and α particles and the effective charge state for α particles, and it is found that the linear response theory can be used to predict the stopping power in a wider energy range if the mean steady-state charge is used instead of assuming fully ionized charges.

I. INTRODUCTION

The energy loss of charged particles in matter has been studied for decades. The study of the interaction between energetic charged particles and matter is the basis for understanding the irradiation effects in materials, which is of great importance in many fields ranging from condensed matter physics to materials science and radiotherapy [1–3]. The energy loss of energetic ions in matter is typically tabulated and parametrized as a quantity called stopping power in units of energy per distance, which is generally divided into two categories depending on the type of excitation produced: (i) elastic collisions between ions and host nuclei that cause displacement damage, referred to as nuclear stopping power S_n [4,5]; and (ii) inelastic collisions between ions and host electrons that lead to electronic excitation and ionization, referred to as electronic stopping power S_e. Compared with the nuclear stopping, the electronic stopping presents additional challenges due to its quantum mechanical nature [6]. Over the past few decades, it has been a subject of great interest to theoretical and experimental physicists to study the electronic stopping power of materials which dominates the energy loss of impinging ions [7–9].

In order to describe the electronic stopping quantitatively and reveal the mechanism responsible for the energy loss, a host of theoretical models have been proposed. The Coulomb scattering formula of Rutherford [10], Thomson [11], and Darwin [12] is of great significance for understanding the stopping power, and it is found that the collision parameter plays an important role in ion-matter interaction. Bethe carried out a consistent quantum-mechanical study and obtained a fundamental equation to describe the stopping of fast charged particles moving in a quantized medium [13]. The free-electron gas (FEG) model proposed by Fermi and Teller [14] showed that the S_e is to be proportional to the projectile velocity for $v < v_0$ (v_0 is the Bohr velocity),

$$S_e = Q(Z_1, r_s)v, \tag{1}$$

where Q is referred to as the friction coefficient of the FEG model. The Q value depends on the atomic number of the projectiles (Z_1) and the Wigner-Seitz radius (r_s) of the FEG. Lindhard and Winther evaluated the electronic stopping within linear response theory based on the dielectric function for the FEG model of a given effective density [15]. The static shielding of protons in an electron gas was calculated by employing density functional theory (DFT), displaying the limitations of the linear response treatment [16,17]. Echenique *et al.* [18,19] proposed a completely nonlinear

treatment method to calculate the electronic stopping power of the FEG model based on DFT calculation, which reproduces the experimental features not captured in the linear response theory calculations.

Although an extensive amount of interesting studies have been focused on the issue of S_e with linear response theory [20–26] and nonlinear formalism [27–33], many of these approaches are limited to the FEG model and do not consider important characteristics, such as the lattice structure and the electronic structure of the substances, and the charge exchange between the projectile ions and the host atoms. These features are becoming especially important at low velocities. The emergence of real-time time-dependent density functional theory (RT-TDDFT) has showed many meaningful advantages in describing the excited electron dynamics under ion irradiation.

Early measurements of the electronic stopping power of metals for slow ions showed deviations from the velocity proportionality in the low-energy region [34–36], which is not consistent with the FEG predictions. In subsequent studies, Valdés *et al.* [37] proposed that the contribution of d-electron excitation is responsible for the deviations from the velocity proportionality of the measured electronic stopping power of copper, silver, and gold for slow protons. Recently, experimental studies on the electronic stopping power [9,38–40] provided detailed evidence for this departure and confirmed the d-electron excitation is responsible for the deviations. It has been observed that the S_e of insulators [41], semiconductors [42], and noble metals [43–46] deviates from the velocity proportionality or vanishes below the threshold velocity due to the band structure effects. The electronic stopping power of LiF and AlF$_3$ with a large band gap was found to vanish below a threshold velocity $v_{th} = 0.10$ a.u. [47]. The threshold effect on the S_e of oxides for slow protons was also experimentally observed [42]. In particular for ZnO, in addition to the threshold velocity, the results also displayed that the electronic stopping rises with a steeper slope due to the contribution from the full d band at $v > 0.25$ a.u. The S_e of Au [43], Ag [44], Cu [45], and Pt [46] for slow light ions exhibits deviations from velocity proportionality when the projectile velocity exceeds the threshold for excitation of inner electrons. Similarly, Goebl *et al.* [48] found experimentally that, due to the excitation threshold of the d band, the friction coefficient Q of indium for protons and He ions increases noticeably at ion velocities 0.20 and 0.25 a.u., respectively.

However, a nonlinear behavior observed in aluminum is interpreted as an additional contribution from the charge exchange between He ions and Al in the low-energy range [49]. Complementary studies using Auger electron spectroscopy showed that, for He ions the formation of molecular orbital leads to excitation of inner shells, thereby opening an additional energy dissipation channel [50]. Wilhelm *et al.* [51] measured the energy loss of slow highly charged Xe ions transmitted through ultrathin carbon membranes, and found that the energy loss is strongly related to the charge loss and the incident charge state of ions. By quantifying the velocity-dependent steady-state charge of the projectile proton and α particle from nonequilibrium simulations, the velocity regime within which linear response treatments are appropriate for describing the electronic stopping power of

silicon carbide [52] and liquid water [53] was examined. These results showed that the description of charge exchange is required for a deeper understanding of the microcosmic mechanism for the energy loss of ions.

At higher velocities, the contribution of inner shell electron excitation to S_e has attracted much attention in recent years. In particular, the degree to which the medium- and high-energy S_e obtained from theoretical calculations is consistent with the experimental results or SRIM predictions is dominated by whether sufficient core electrons are considered. Recently, Lohmann and Primetzhofer [54] measured the electronic stopping power of protons and He ions moving along the channeling and off-channeling trajectories in silicon, and the relative contribution of core electron excitation to S_e was qualitatively given, which is of great significance for further understanding the contribution of core electron excitation. Quashie *et al.* [55] investigated the stopping power of crystalline Cu for protons based on TDDFT combined with a pseudopotential scheme, and the results showed that the core electron excitation makes a crucial contribution to medium- and high-energy S_e. The study of the S_e of nickel for protons and α particles also suggested that the inner electrons of the host play an important role in the high-energy stopping power [56].

It is extremely important to study the excitation behavior of semicore electrons, and crystalline indium is chosen as the research object of the present study. In this paper, we investigated the S_e of indium for channeling and off-channeling protons and He ions based on RT-TDDFT, respectively. The deviations from the velocity-proportional S_e of indium are reproduced in the low-velocity regime and the contribution of $4d$-electron excitation to the S_e is studied in a wide velocity range. In addition, we discussed the applicability of the linear response theory in the low-energy range and mean steady-state charge of projectile ions and the effective charge for α particles.

II. METHOD AND COMPUTATIONAL DETAILS

Ehrenfest molecular dynamics combined with the time-dependent density functional theory (EMD-TDDFT) model [57–59] is employed to study the stopping of protons and He ions in In. The combined application of time-dependent density functional theory calculations for electrons and molecular dynamics [60–62] simulations for ions makes it possible to study the nonequilibrium response of the electronic subsystem of the target medium to energetic ions, and to calculate the nonadiabatic energy exchange between the energetic ions and the host electrons [63]. This method allows for excited electronic states *ab initio* molecular dynamics simulation. The EMD scheme is defined by the following equations (atomic units are used hereafter):

$$M_I \ddot{\mathbf{R}}_I = -\sum_{I \neq J} \nabla_I \frac{Z_I Z_J}{|\mathbf{R}_I(t) - \mathbf{R}_J(t)|}$$

$$-\int \Psi^*(x,t) \nabla_I \hat{H}_e[r, R(t)] \Psi(x,t) dx, \quad (2)$$

$$i \frac{\partial \Psi(x,t)}{\partial t} = \hat{H}_e[r, R(t)] \Psi(x,t), \quad (3)$$

where $\Psi(x, t)$ is the many-body wave function of the noninteracting electrons. $\hat{H}_e[r, R(t)]$ is the electronic Hamiltonian, $R(t) \equiv \{\mathbf{R}^M(t)\}$ is the instantaneous position of all the nuclei, and M is the number of nuclei in the system. The mass and charge of the Ith nucleus are expressed as M_I and Z_I, respectively. The motion of the nuclei is determined by the set of Eq. (2). The electronic Hamiltonian is defined as

$$\hat{H}_e[r, R(t)] = -\sum_{i=1}^{N} \frac{1}{2}\nabla_i^2 + \sum_{i<j} \frac{1}{|\mathbf{r}_i - \mathbf{r}_j|} - \sum_{Ii} \frac{Z_I}{|\mathbf{R}_I(t) - \mathbf{r}_i|}. \tag{4}$$

N is the number of electrons in the system. This form of the Hamiltonian allows one to write the force that acts on each nucleus solely in terms of the electronic density $\rho(\mathbf{r},t)$. Therefore, instead of solving Eq. (3), the evolution of electron density and energy during the collision between projectile ions with solid targets can be described by solving the time-dependent Kohn-Sham equation:

$$i\frac{\partial \varphi_i(\mathbf{r}, t)}{\partial t} = \left[-\frac{1}{2}\nabla^2 - \sum_I \frac{Z_I}{|\mathbf{R}_I(t) - \mathbf{r}|} + \int d\mathbf{r}' \frac{\rho(\mathbf{r}', t)}{|\mathbf{r} - \mathbf{r}'|} \right. $$
$$\left. + V_{\text{XC}}(\mathbf{r}, t) \right] \varphi_i(\mathbf{r}, t) \tag{5}$$

and

$$\rho(\mathbf{r}, t) = 2 \sum_{i=1}^{N/2} |\varphi_i(\mathbf{r}, t)|^2. \tag{6}$$

Here, $\varphi_i(\mathbf{r}, t)$ is the time-dependent Kohn-Sham single-electron orbital. The four terms on the right-hand side of Eq. (5) are the electron kinetic, the time-dependent electron-nucleus, classic Hartree, and exchange-correlation potentials, respectively.

In this theoretical framework, the interaction between electrons and ionic cores is described by the norm-conserving Troullier-Martins pseudopotential [64]. The adiabatic local density approximation with Perdew-Wang parametrization [65] for the exchange-correlation (XC) potential is employed in the time-evolving calculations. In order to develop the ionic movements, the Verlet algorithm is used for the integration of the ion motion equation, and the approximate forced time antisymmetry method is used for propagating the electronic wave function. In order to clarify the excitation effect of semicore $4d$ electrons on the electronic energy loss of ions, we constructed two pseudopotential models with 3 and 13 valence electrons for the indium atom, which are labeled as In3 ([Xe$4d^{10}$]$5s^2 5p^1$) and In13 ([Xe]$4d^{10}5s^2 5p^1$) in the present study, respectively.

A $3 \times 3 \times 3$ supercell containing 54 indium atoms is employed in the present study, and the periodic boundary conditions and Ewald summation are considered. The wave functions, electron densities, and external potentials are discretized in a real-space grid with uniform spacing of 0.16 Å along all three spatial coordinates in the simulation cell. Before the time-dependent evolution, the electronic ground state for indium is achieved by diagonalization of the time-independent Kohn-Sham Hamiltonian. The projectiles are initially placed on the boundary of the simulation cell at the
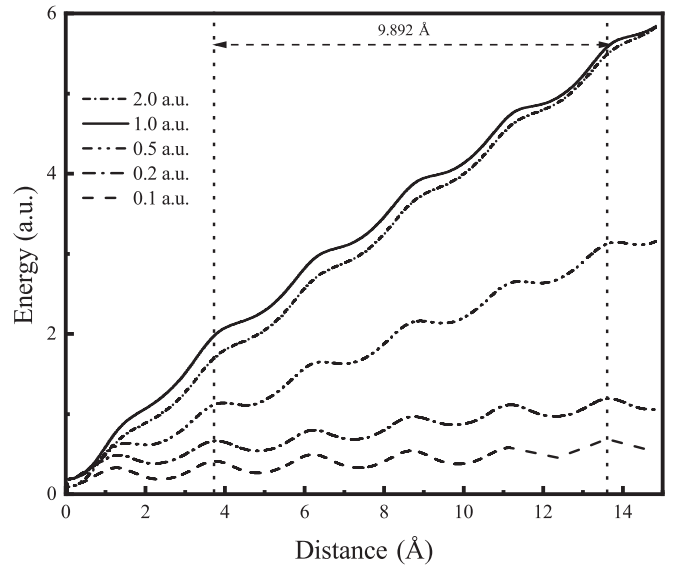

FIG. 1. Total energy increment as a function of proton position in the channeling trajectory B for various velocities.

beginning of the time evolution. In the real-time evolution, the protons and α particles are constrained to move along straight trajectories in both channeling and off-channeling geometries, and the host atoms are held fixed at their equilibrium positions [52,56]. So, the projectile energy is transferred only to the electronic subsystem of indium through inelastic collisions. The projectiles are forced to keep constant velocity in the simulations, therefore leading to the total energy of the system increasing with the projectile displacement since the projectile deposits energy into the electronic subsystem as it moves through indium. We set different propagation step lengths so that $\Delta t \times v \sim 3.455 \times 10^{-3}$ Å for various velocities, which is used to ensure the convergence of the total energy. Figure 1 shows the total energy increment of the projectile-target system as a function of position for different velocities in the channeling geometry. This allows us to directly determine the instantaneous electronic stopping power. However, it is worth noting that the sudden entrance of the projectile and the charge exchange between the impact ions and indium cause a "transient" in the total energy of the system [55,66], which is significant in the low-energy region. To avoid the effect of the "transient" on the stopping power, we extracted the instantaneous electronic stopping power after the ions reach an equilibrium charged state [66]. The equilibrium electronic stopping power is obtained by averaging the instantaneous electronic stopping power over two lattice periods between the two vertical dashed lines as indicated in Fig. 1. In order to investigate the influences of the impact parameter on the electronic stopping power, we calculated the electronic stopping power of projectiles traveling along the c axis in two channeling trajectories depending on the impact parameter. The incident points for trajectories A and B are shown in the insets of Figs. 2 and 3, respectively.

The projectiles pass through the host material in random directions in the off-channeling geometry, and they occasionally interact strongly with the tightly bound electrons of the host atoms. For the off-channeling geometry, different
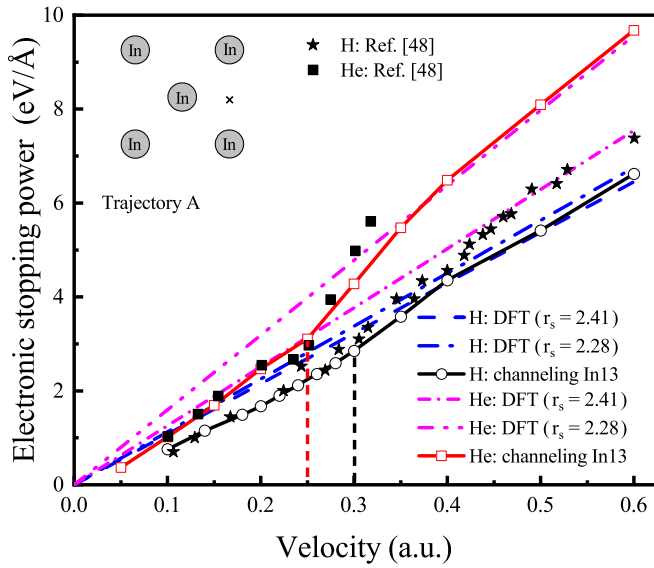
FIG. 2. Electronic stopping power of indium including also $4d$ electrons as a function of velocity for H and He ions moving along the channeling trajectory A. Experimental data from Ref. [48] are presented. FEG predictions based on DFT calculation for H [69] and He [28,70] ions are also displayed. The short dash lines are to guide the eye. The inset shows the top view of the incidence geometry. The gray circles represent the indium atoms, and the black fork indicates the impact location of the projectiles.
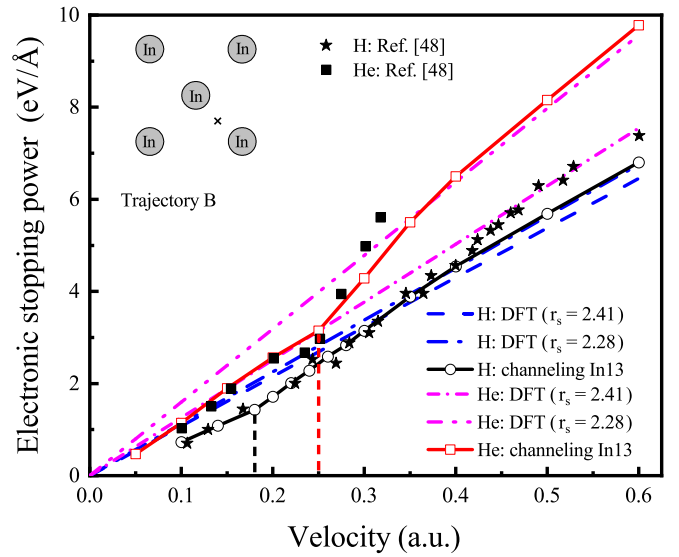

FIG. 3. Electronic stopping power of indium including also $4d$ electrons as a function of velocity for H and He ions moving along the channeling trajectory B. Experimental data from Ref. [48] are presented. FEG predictions based on DFT calculation for H [69] and He [28,70] ions are also displayed. The short dash lines are to guide the eye. The inset shows the top view of the incidence geometry. The gray circles represent the indium atoms, and the black fork indicates the impact location of the projectiles.

incidence positions and directions are chosen to sample all possible impact parameters, and head-to-head collision between the ion and the host atoms is avoided. Three incident directions [0.304, 0.047, 0.952], [0.317, 0.320, 0.893], and [0.444, 0.513, 0.735] are selected following Ref. [55] (given normalized here). Three initial positions are selected for each incident direction, so there are nine off-channeling trajectories for each velocity. The off-channeling stopping power is obtained by averaging the stopping results of the nine trajectories for each velocity. In addition, the excitation of plasmons with wavelengths longer than the simulation cell cannot be described correctly, which may underestimate the electronic stopping power at high velocities. Therefore, the finite size effects were studied by a larger supercell ($4 \times 4 \times 4$) including 128 indium atoms, for selected velocities with negligible difference within 2.8%. The calculations are performed by OCTOPUS code [67,68].

III. RESULTS AND DISCUSSION

Figure 2 shows our RT-TDDFT S_e results of indium for H and He projectiles moving along the channeling trajectory A in the low-velocity range, along with the experimental data [48]. Also shown are the FEG predicted S_e based on DFT calculation with Wigner-Seitz radius $r_s = 2.28$ a.u. ($4d^{10}5s^25p^1$) and $r_s = 2.41$ a.u. ($5s^25p^1$) for H [69] and He [28,70] ions. For both projectiles, deviations from the velocity proportionality of the electronic stopping power of indium [48] are reproduced by our RT-TDDFT calculations in the low-energy region. It can be seen from the figure that the stopping power curve is divided into three velocity proportionality regions

by two velocity points. For protons, the velocity-proportional stopping power is reproduced at $v < 0.30$ a.u. In this regime, the projectiles interact exclusively with the $5s5p$ valence electrons of the host atoms. In the second regime 0.30 a.u. $< v < 0.40$ a.u., the S_e data deviate from the velocity proportionality with a steeper slope due to the excitation of the $4d$-band electron. The velocity for the transition between the two velocity scaling regimes is referred to as kink velocity v_k. So, our calculated v_k is 0.30 a.u. for protons in this trajectory, which is higher than the measured value 0.20 a.u. [48]. The S_e displays the linear-velocity dependence again at $v > 0.40$ a.u. Our stopping power results are consistent with the experimental data but are lower than the FEG predictions at $v < 0.40$ a.u. At velocities > 0.40 a.u., our RT-TDDFT simulation results slightly underestimate the experimental data [48] (the calculated S_e is lower than the experimental one by 7.4% at 0.60 a.u.), but approach the FEG predictions with $4d$ electrons considered.

For He ions, two deviations from the velocity proportionality are found. The calculated S_e exhibits velocity proportionality up to ion velocity ≈ 0.25 a.u. The slope of the stopping power increases noticeably due to the contribution of $4d$-electron excitation of indium at velocities between 0.25 and 0.35 a.u. So, the obtained v_k is 0.25 a.u. for He ions in this channeling geometry, which is in pretty good agreement with the experimental value 0.25 a.u. The general agreement between our RT-TDDFT calculations and the FEG predictions is pretty good except for the crossover regime 0.25 a.u. $< v < 0.35$ a.u. The linear velocity dependence of S_e is achieved again at velocities larger than 0.35 a.u. The agreement between our data and the DFT results for the FEG model with $r_s = 2.41$ a.u. is excellent below 0.25 a.u. At

$v > 0.25$ a.u., our RT-TDDFT simulation results are lower than the experimental data; while they are in excellent agreement with the FEG predictions with $4d$ electrons taken into account at $v > 0.35$ a.u.

In order to understand the dependence of S_e on the impact parameter, the S_e of indium for ions moving along trajectory B is shown in Fig. 3. The three velocity-proportional regions of S_e are still present for both projectiles moving along this channeling geometry, as shown in Fig. 3. For protons, our RT-TDDFT results exhibit a velocity-proportional behavior up to 0.18 a.u. In the velocity regime 0.18 a.u. $< v < 0.35$ a.u. the stopping power shows a higher slope than the aforementioned region due to the additional excitation of the $4d$-band electrons. At $v > 0.35$ a.u., the linear electronic stopping power is quite consistent with the predictions given by FEG corresponding to $r_s = 2.28$ a.u. Our results are in fair agreement with the experimental data at $v < 0.40$ a.u. The channeling stopping is lower than the measured value by 5.3% at 0.60 a.u. In this channeling trajectory the v_k is 0.18 a.u., which is slightly lower than the experimental value 0.20 a.u. The v_k values for protons channeling in the two trajectories are different, which suggests that the excitation of the $4d$ electrons is related to the impact parameter. In our RT-TDDFT calculations, the S_e and v_k for slow He ions traveling in trajectory B are consistent with those in trajectory A.

In fact, the threshold velocity for excitation of the $4d$ electrons to the Fermi level can be calculated by the following equation:

$$v_k = \frac{E_d}{2\hbar k_F}, \quad (7)$$

where E_d represents the $4d$-band offset, which is the energy interval between the edge of the $4d$ band and the Fermi energy level of In. The DFT calculation of E_d is 14.29 eV in the present study, which is smaller than the experimental value $E_d = 16$ eV. The Fermi wave vector $k_F = 1.92/r_s$ is for uniform electron gas of In $5s5p$ electrons ($r_s = 2.41$ a.u.). According to Eq. (7), the calculated kink velocity $v_k = 0.33$ a.u. is higher than the experimental values and our RT-TDDFT results.

The S_e of indium for protons and He ions is extended to 6.0 a.u., and the results are shown in Fig. 4. Due to the lack of experimental data in the high-energy region, our RT-TDDFT simulation results are compared with the SRIM predictions [71]. The SRIM model is based on the extended Lindhard-Scharff-Schiøtt theory [72] with inputs from available experiments, and the stopping power predictions given by SRIM are widely used as a standard reference. For both projectiles, the S_e considering only valance electrons ($5s5p$) for ions moving along the two channeling trajectories is almost consistent in the low-velocity range. This is due to the fact that the valence electrons are homogeneously distributed inside the target and even within the channel, and the energy loss mainly stems from the excitation of valence electrons via Coulomb scattering. Thus, a marginal difference of S_e between the two channeled trajectories is expected. In contrast, the stopping power including also $4d$ electrons obtained from trajectory B is significantly higher than that in trajectory A, especially at $v > 1.0$ a.u., which demonstrates that the excitation of semicore electrons is highly dependent on the impact parameter
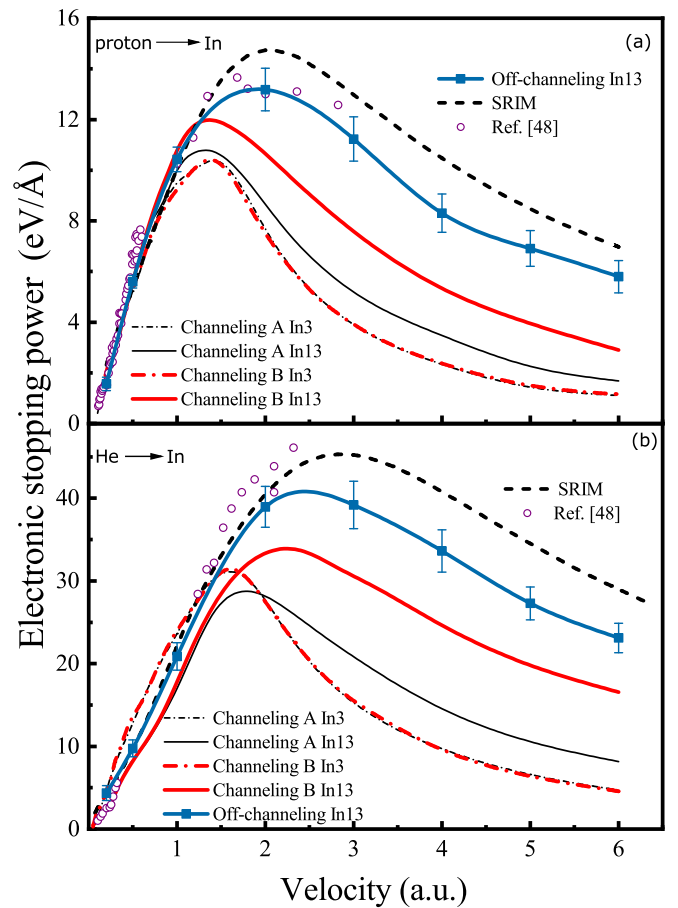

FIG. 4. Electronic stopping power of In for (a) protons and (b) He ions versus projectile velocity. The red and black lines represent the RT-TDDFT simulation results for the projectiles channeling along trajectory A and B, respectively. The solid and short dash–dotted lines indicate the results with $4d$ electrons considered or not, respectively. Blue squares display the results obtained from off-channeling trajectories. The purple circles denote the experimental measurements [48]. The dashed line is the stopping power values predicted by the SRIM package.

and suggests that ion-electron collision is responsible for the excitation of the highly localized $4d$ electrons. This is also verified by calculating the radial distribution of electron density of the channeling trajectory. The results showed that the electron density of trajectory B is higher than that of trajectory A. For protons, the channeling stopping without $4d$ electrons is lower than the SRIM data by 83.4% at $v = 6.0$ a.u. However, the underestimation of S_e obtained from trajectories A and B is reduced to 75.7% and 58.3% with the semicore electron excitation considered, respectively.

For He ions, the channeling stopping power of indium containing only $5s5p$ electrons is lower than the SRIM value by 83.5% at $v = 6.0$ a.u. However, the channeling S_e including also $4d$-electron excitation contribution is increased by 44.1% and 72.4% in trajectory A and B, respectively. In general, the electronic stopping power obtained from the channeling trajectories is lower than the experimental values and SRIM data in the high-energy region. This is because the projectiles traverse along random trajectories in the target in experiments,

occasionally resulting in a stronger interaction between the projectile and the tightly bound electrons in close collisions. It can be seen from Fig. 4 that the position of the Bragg peak is related to the number of electrons participating in the stopping dynamics.

Considering the higher excitation efficiency of inner electrons in the off-channeling geometry, the off-channeling stopping including also $4d$ electrons is calculated. Compared with the channeling results, the off-channeling S_e is significantly improved at high velocities, approaching the SRIM results. For protons, the off-channeling S_e is in good agreement with experimental data up to 2.0 a.u., and it is consistent with the experimental data near the stopping maximum. Moreover, the off-channeling S_e displays a higher semicore electron excitation efficiency in comparison with the channeling case beyond 1.2 a.u. Compared with the channeling stopping, the off-channeling S_e for protons is greatly improved and it is lower than the SRIM result by only 15.5% at 6.0 a.u.

For He ions, the agreement between the off-channeling stopping power and the measured data is achieved up to 2.0 a.u., while our off-channeling results are lower than the experimental data and SRIM predictions at velocities beyond 2.0 a.u. The off-channeling stopping power is increased by 39.6% in comparison with that including also $4d$ electrons obtained from trajectory B at 6.0 a.u. It can be derived from Fig. 4(b) that, the energy loss of He ions traversing through trajectory B and off-channeling geometry cases is dominated by $4d$-electron excitation in the high-energy region. The off-channeling stopping power of protons and He ions deviates from the SRIM results at $v = 1.2$ and 1.4 a.u., respectively, indicating more electrons are required to be incorporated in the stopping of indium.

Many studies showed that the charge transfer is an important energy loss channel in the low-energy range [51,73–75]. The difficulty for extracting charge transfer is to distinguish the electron density of the ions from the medium [52,53,73]. A reasonable partitioning scheme is employed to quantify the nonequilibrium electron density border between the ions and the host atoms in our RT-TDDFT simulations. The electronic charges carried by the projectiles are considered to be distributed in spheres, and the ion position is the center of the spheres. The sphere is divided into many equally spaced sphere shells, and the shell thickness is 0.08 Å in the present study. The sphere shell with the lowest electron density is considered as the border for the electron density between the ions and host atoms. Using this method, the integration radius for He ions and protons is chosen as 0.88 and 0.80 Å, respectively, and the charges captured by the projectiles are obtained by integrating the electron density within the spheres. In order to quantify the charge state of the projectile ion throughout the entire trajectory, 45 equally spaced electron density "snapshots" were taken from the trajectory for each velocity. The mean charge captured by the ions is obtained by averaging the 45 charges at different positions of the trajectory. The advantage of this method is that it provides insight into the dynamics of the charge capture and loss, and allows the calculation of the mean steady-state charge.

Considering that the number of electrons captured by the projectiles is different only in magnitude under different channeling trajectories and it does not affect the qualitative
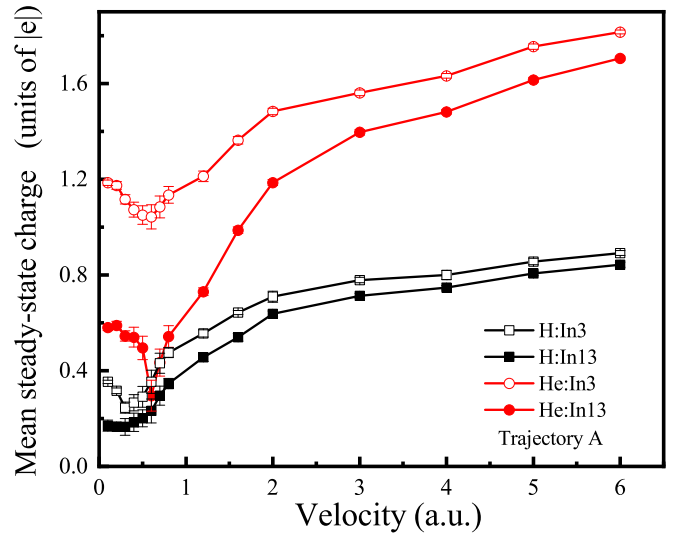

FIG. 5. The mean steady-state charge as a function of velocity for protons (black squares) and He ions (red circles). Solid and empty squares indicate the results with $4d$ electrons considered or not, respectively. All the results here are obtained from the channeling trajectory A.

analysis, we only give the mean steady-state charge ($\bar{q}$) of H and He ions as a function of velocity for the channeling trajectory A, as shown in Fig. 5. The mean steady-state charge of the ions increases as the ion velocity $v > 0.50$ a.u., and the projectiles approach the fully ionized state at high velocities. It is noted that the steady charge state of He ions in the In3 model is much higher than that in the In13 model in the low-velocity range, which gives rise to the channeling stopping power without $4d$ electrons is higher than the channeling and off-channeling stopping power including also $4d$ electrons for $v < 1.5$ a.u., as shown in Fig. 4(b). In the framework of linear response theory, assuming the projectiles are completely ionized, the stopping force between ions with fixed charge and matter is quadratic dependent on the charge of the ions. The extent to which the linear response theory can be employed to describe the electronic stopping power without higher order correction, and whether the description can be improved if the velocity-dependent mean steady-state charge of the ions obtained from our nonequilibrium simulation is used instead of fully ionized projectile ions. These questions are answered in the following discussion.

Based on the mean steady-state charge and electronic stopping power discussed above, the comparison of the square root of the stopping power ratio sqrt[S_α/S_H] to the mean steady-state charge ratio $\bar{q}_\alpha/\bar{q}_H$ is shown as a function of velocity in Fig. 6. Since the effective charge of ions is defined as $Z_{eff} = [S_{ion}/S_H]^{1/2}$, the sqrt[$S_\alpha/S_H$] corresponds to the effective charge of He ions. The sqrt[S_α/S_H] reaches 2 beyond 3.0 a.u., as one would expect from assuming fully ionized charges in the linear response theory (i.e., sqrt[S_α/S_H] = Z_α/Z_H). Our RT-TDDFT simulation and experimental results showed that the sqrt[S_α/S_H] is less than 2 at $v < 3.0$ a.u., because the linear response theory begins to fail at lower velocities. For both pseudopotentials, the sqrt[S_α/S_H] obtained from the two channeling trajectories is consistent in the studied velocity
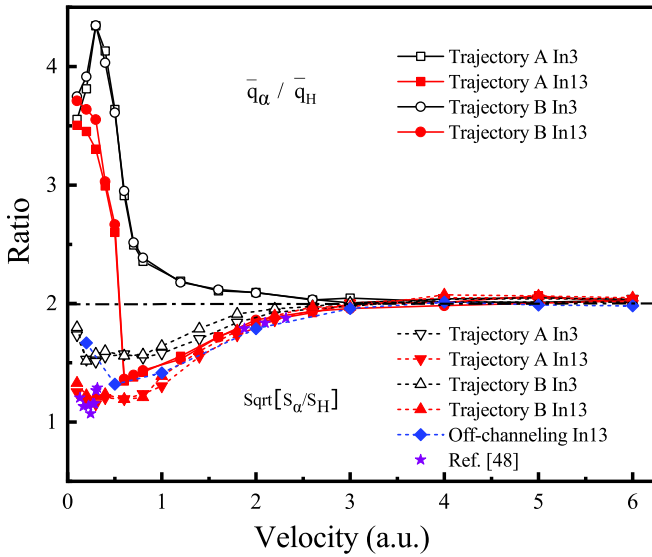
FIG. 6. Velocity-dependent ratios between α particles and protons for stopping power and mean steady-state charge in indium. Squares and circles show the $\bar{q}_\alpha/\bar{q}_H$ obtained from trajectories A and B, and full and open symbols indicate the $\bar{q}_\alpha/\bar{q}_H$ with $4d$ electrons considered or not, respectively. The effective charge state sqrt[S_α/S_H] is calculated from the stopping power ratio between α particles and protons. The inverted and the regular triangles show the sqrt[S_α/S_H] obtained from trajectories A and B, and the full and open symbols indicate the sqrt[S_α/S_H] including also $4d$ electrons or not, respectively. Diamonds represent sqrt[S_α/S_H] calculated from off-channeling trajectories. Pentagrams denote sqrt[S_α/S_H] derived from the experimental data [48]. The dash-dotted line represents the stopping power ratio of 2, which is expected from linear response theory when assuming fully ionized charges.

range, with negligible differences at velocities below 0.5 a.u., as well as $\bar{q}_\alpha/\bar{q}_H$. These results showed that both sqrt[S_α/S_H] and $\bar{q}_\alpha/\bar{q}_H$ are related to the pseudopotential model and independent of the impact parameter. However, the sqrt[S_α/S_H] given by the In3 pseudopotential model is higher than that given by the In13 pseudopotential model at $v \leqslant 2.6$ a.u., which is becoming significant at lower velocities. For the off-channeling trajectory, our calculations showed that the sqrt[S_α/S_H] reaches 2 beyond 3.0 a.u., and it is consistent with the results obtained from the In13 pseudopotential model and the experimental data down to 0.5 a.u. In the low-energy range, the $\bar{q}$ of He ions obtained from the In3 pseudopotential model is higher in comparison with the In13 pseudopotential model, while the $\bar{q}$ of protons are very close in the two pseudopotential models. This leads to significant differences for both $\bar{q}_\alpha/\bar{q}_H$ and sqrt[S_α/S_H] obtained from the two pseudopotential models in the low-velocity region.

Returning to the question of the relationship between the effective charge Z_{eff} for α particles and the ratio of mean steady-state charge between α particles and protons, it is interesting to examine the extent to which the two quantities become equivalent. For the In3 model, the two quantities are in perfect agreement at velocities beyond 2.6 a.u., but there is

a significant difference between the two quantities at $v < 2.6$ a.u. For the In13 model, sqrt[S_α/S_H] follows rather closely to the ratio $\bar{q}_\alpha/\bar{q}_H$ even at low ion velocities down to 0.6 a.u. Therefore, this suggested that the linear response theory can give a reasonable prediction of the electronic stopping over a wide velocity range if the mean steady-state charge is used instead of assuming fully ionized charges and considering also $4d$-electron excitation. From a numerical point of view, the consideration of semicore electron excitation is very important for the equivalence between the two quantities at low velocities.

IV. CONCLUSIONS

In this paper, we reported the electronic stopping power of indium for energetic protons and He ions based on real-time time-dependent density functional theory. For both projectiles, the experimentally observed deviations from velocity proportionality of the electronic stopping power are reproduced. Our RT-TDDFT channeling stopping power for protons underestimates the experimental data beyond 0.4 a.u., and the channeling stopping power for He ions deviates from the experimental data towards lower values above 0.25 a.u. However, the off-channeling stopping is greatly improved and it is in good agreement with the experimental values up to 2.0 a.u. for both projectiles. Our results demonstrated that the excitation of valence electrons is independent of the impact parameter which is triggered by Coulomb scattering, and the excitation of semicore $4d$ electrons is strongly dependent on the impact parameter which suggests the excitation of semicore $4d$ electrons is attributed to direct ion-electron collision. Our results showed that the $4d$-electron excitation contributes substantially to the electronic stopping power of indium in the high-energy range.

The mean steady-state charge of the ions channeling in indium is studied in the present work, and the shielding effect of semicore electrons is verified. The ratio of the mean steady-state charge of the projectiles is calculated and a comparison between $\bar{q}_\alpha/\bar{q}_H$ and sqrt[S_α/S_H] is given. It is pointed out that the effective charge Z_{eff} for α particles and the ratio of mean steady-state charge $\bar{q}_\alpha/\bar{q}_H$ are related to the number of electrons involved in the stopping dynamics, and are independent of the impact parameter. With considering also the $4d$-electron excitation of indium, the validity of the linear response theory for describing the stopping power is extended to lower velocities if the mean steady-state charge is used instead of assuming fully ionized charges.

[1] S. J. Zinkle, V. A. Skuratov, and D. T. Hoelzer, Nucl. Instrum. Methods Phys. Res., Sect. B **191**, 758 (2002).

[2] L. Moroz, G. Baratta, G. Strazzulla, L. Starukhina, E. Dotto, M. A. Barucci, G. Arnold, and E. Distefano, Icarus **170**, 214 (2004).

[3] G. J. Caporaso, Y.-J. Chen, and S. E. Sampayan, Rev. Accel. Sci. Technol. **2**, 253 (2009).

[4] M. T. Robinson and I. M. Torrens, Phys. Rev. B **9**, 5008 (1974).

[5] K. Arstila, J. Keinonen, P. Tikkanen, and A. Kuronen, Phys. Rev. B **43**, 13967 (1991).

[6] G. Schiwietz and P. L. Grande, Phys. Rev. A **84**, 052703 (2011).

[7] M. Inokuti, Rev. Mod. Phys. **43**, 297 (1971).

[8] P. E. Grabowski, M. P. Surh, D. F. Richards, F. R. Graziani, and M. S. Murillo, Phys. Rev. Lett. **111**, 215002 (2013).

[9] E. A. Figueroa, E. D. Cantero, J. C. Eckardt, G. H. Lantschner, J. E. Valdés, and N. R. Arista, Phys. Rev. A **75**, 010901(R) (2007).

[10] E. Rutherford, London, Edinburgh Dublin Philos. Mag. J. Sci. **21**, 669 (1911).

[11] J. J. Thomson, London, Edinburgh Dublin Philos. Mag. J. Sci. **23**, 449 (1912).

[12] C. G. Darwin, London, Edinburgh Dublin Philos. Mag. J. Sci. **23**, 901 (1912).

[13] H. Bethe, Ann. Phys. **397**, 325 (1930).

[14] E. Fermi and E. Teller, Phys. Rev. **72**, 399 (1947).

[15] J. Lindhard and A. Winther, *Stopping Power of Electron Gas and Equipartition Rule* (Munksgaard, Copenhagen, 1964).

[16] C. O. Almbladh, U. von Barth, Z. D. Popovic, and M. J. Stott, Phys. Rev. B **14**, 2250 (1976).

[17] E. Zaremba, J. H. Rose, L. M. Sander, and H. B. Shore, J. Phys. F: Met. Phys. **7**, 1763 (1977).

[18] P. M. Echenique, R. M. Nieminen, and R. H. Ritchie, Solid State Commun. **37**, 779 (1981).

[19] P. M. Echenique, R. M. Nieminen, J. C. Ashley, and R. H. Ritchie, Phys. Rev. A **33**, 897 (1986).

[20] R. H. Ritchie, Phys. Rev. **114**, 644 (1959).

[21] W. Brandt and J. Reinheimer, Phys. Rev. B **2**, 3104 (1970).

[22] T. Kaneko, Phys. Status Solidi B **156**, 49 (1989).

[23] J. J. Dorado and F. Flores, Phys. Rev. A **47**, 3062 (1993).

[24] I. Abril, R. Garcia-Molina, C. D. Denton, F. J. Peŕez-Peŕez, and N. R. Arista, Phys. Rev. A **58**, 357 (1998).

[25] I. Campillo, J. M. Pitarke, and A. G. Eguiluz, Phys. Rev. B **58**, 10307 (1998).

[26] J. M. Pitarke and I. Campillo, Nucl. Instrum. Methods Phys. Res., Sect. B **164-165**, 147 (2000).

[27] T. L. Ferrell and R. H. Ritchie, Phys. Rev. B **16**, 115 (1977).

[28] M. J. Puska and R. M. Nieminen, Phys. Rev. B **27**, 6121 (1983).

[29] B. Apagyi and I. Nagy, J. Phys. C: Solid State Phys. **20**, 1465 (1987).

[30] A. F. Lifschitz and N. R. Arista, Phys. Rev. A **57**, 200 (1998).

[31] A. Salin, A. Arnau, P. M. Echenique, and E. Zaremba, Phys. Rev. B **59**, 2537 (1999).

[32] J. I. Juaristi, C. Auth, H. Winter, A. Arnau, K. Eder, D. Semrad, F. Aumayr, P. Bauer, and P. M. Echenique, Phys. Rev. Lett. **84**, 2124 (2000).

[33] N. R. Arista, Nucl. Instrum. Methods Phys. Res., Sect. B **195**, 91 (2002).

[34] R. Blume, W. Eckstein, and H. Verbeek, Nucl. Instrum. Methods Phys. Res. **168**, 57 (1980).

[35] R. Blume, W. Eckstein, and H. Verbeek, Nucl. Instrum. Methods Phys. Res. **194**, 67 (1982).

[36] J. E. Valdés, G. Martińez Tamayo, G. H. Lantschner, J. C. Eckardt, and N. R. Arista, Nucl. Instrum. Methods Phys. Res., Sect. B **73**, 313 (1993).

[37] J. E. Valdés, J. C. Eckardt, G. H. Lantschner, and N. R. Arista, Phys. Rev. A **49**, 1083 (1994).

[38] E. D. Cantero, G. H. Lantschner, J. C. Eckardt, and N. R. Arista, Phys. Rev. A **80**, 032904 (2009).

[39] S. N. Markin, D. Primetzhofer, S. Prusa, M. Brunmayr, G. Kowarik, F. Aumayr, and P. Bauer, Phys. Rev. B **78**, 195122 (2008).

[40] D. Roth, B. Bruckner, M. V. Moro, S. Gruber, D. Goebl, J. I. Juaristi, M. Alducin, R. Steinberger, J. Duchoslav, D. Primetzhofer, and P. Bauer, Phys. Rev. Lett. **118**, 103401 (2017).

[41] S. N. Markin, D. Primetzhofer, and P. Bauer, Phys. Rev. Lett. **103**, 113201 (2009).

[42] D. Roth, B. Bruckner, G. Undeutsch, V. Paneta, A. I. Mardare, C. L. McGahan, M. Dosmailov, J. I. Juaristi, M. Alducin, J. D. Pedarnig, R. F. Haglund, Jr., D. Primetzhofer, and P. Bauer, Phys. Rev. Lett. **119**, 163401 (2017).

[43] M. A. Zeb, J. Kohanoff, D. Sánchez-Portal, A. Arnau, J. I. Juaristi, and E. Artacho, Phys. Rev. Lett. **108**, 225504 (2012).

[44] D. Goebl, D. Roth, and P. Bauer, Phys. Rev. A **87**, 062903 (2013).

[45] S. N. Markin, D. Primetzhofer, M. Spitz, and P. Bauer, Phys. Rev. B **80**, 205105 (2009).

[46] D. Primetzhofer, Phys. Rev. B **86**, 094102 (2012).

[47] L. N. Serkovic Loli, E. A. Sánchez, O. Grizzi, and N. R. Arista, Phys. Rev. A **81**, 022902 (2010).

[48] D. Goebl, W. Roessler, D. Roth, and P. Bauer, Phys. Rev. A **90**, 042706 (2014).

[49] D. Primetzhofer, S. Rund, D. Roth, D. Goebl, and P. Bauer, Phys. Rev. Lett. **107**, 163201 (2011).

[50] P. Riccardi, A. Sindona, and C. A. Dukes, Phys. Lett. A **381**, 1174 (2017).

[51] R. A. Wilhelm, E. Gruber, R. Ritter, R. Heller, S. Facsko, and F. Aumayr, Phys. Rev. Lett. **112**, 153201 (2014).

[52] D. C. Yost and Y. Kanai, Phys. Rev. B **94**, 115107 (2016).

[53] Kyle G. Reeves, Yi Yao, and Y. Kanai, Phys. Rev. B **94**, 041108(R) (2016).

[54] S. Lohmann and D. Primetzhofer, Phys. Rev. Lett. **124**, 096601 (2020).

[55] E. E. Quashie, B. C. Saha, and A. A. Correa, Phys. Rev. B **94**, 155403 (2016).

[56] E. E. Quashie and A. A. Correa, Phys. Rev. B **98**, 235122 (2018).

[57] X. Andrade, A. Castro, D. Zueco, J. L. Alonso, P. Echenique, F. Falceto, and A. Rubio, J. Chem. Theory Comput. **5**, 728 (2009).

[58] J. L. Alonso, X. Andrade, P. Echenique, F. Falceto, D. Prada-Gracia, and A. Rubio, Phys. Rev. Lett. **101**, 096403 (2008).

[59] A. Castro, M. Isla, J. I. Martínez, and J. A. Alonso, Chem. Phys. **399**, 130 (2012).

[60] J. M. Pruneda, D. Sánchez-Portal, A. Arnau, J. I. Juaristi, and E. A. Artacho, Phys. Rev. Lett. **99**, 235501 (2007).

[61] A. A. Correa, J. Kohanoff, E. Artacho, D. Sánchez-Portal, and A. Caro, Phys. Rev. Lett. **108**, 213201 (2012).

[62] D. R. Mason, J. L. Page, C. P. Race, W. M. C. Foulkes, M. W. Finnis, and A. P. Sutton, J. Phys.: Condens. Matter **19**, 436209 (2007).

[63] M. A. Zeb, J. Kohanoff, D. Sánchez-Portal, and E. Artacho, Nucl. Instrum. Methods Phys. Res., Sect. B **303**, 59 (2013).

[64] N. Troullier and J. L. Martins, Phys. Rev. B **43**, 1993 (1991).

[65] J. P. Perdew and Y. Wang, Phys. Rev. B **45**, 13244 (1992).

[66] A. Schleife, Y. Kanai, and A. A. Correa, Phys. Rev. B **91**, 014306 (2015).

[67] X. Andrade, D. A. Strubbe, U. De Giovannini, A. H. Larsen, M. J. T. Oliveira, J. Alberdi-Rodriguez, A. Varas, I. Theophilou, N. Helbig, M. Verstraete, L. Stella, F. Nogueira, A. Aspuru-Guzik, A. Castro, M. A. L. Marques, and A. Rubio, Phys. Chem. Chem. Phys. **17**, 31371 (2015).

[68] X. Andrade, J. Alberdi-Rodriguez, D. A. Strubbe, M. J. T. Oliveira, F. Nogueira, A. Castro, J. Muguerza, A. Arruabarrena, S. G. Louie, A. Aspuru-Guzik, A. Rubio, and M. A. L. Marques, J. Phys.: Condens. Matter **24**, 233202 (2012).

[69] J. I. Juaristi, M. Alducin, R. Díez Muiño, H. F. Busnengo, and A. Salin, Phys. Rev. Lett. **100**, 116102 (2008).

[70] I. Nagy and A. Arnau, Phys. Rev. B **49**, 9955 (1994).

[71] J. F. Ziegler, M. Ziegler, and J. Biersack, Nucl. Instrum. Methods Phys. Res., Sect. B **268**, 1818 (2010).

[72] J. Lindhard, M. Scharff, and H. E. Schiøtt, *Range Concepts and Heavy Ion Ranges* (Munksgaard, Copenhagen, 1963).

[73] A. Kononov and A. Schleife, Phys. Rev. B **102**, 165401 (2020).

[74] R. Cabrera-Trujillo, J. R. Sabin, Y. Öhrn, and E. Deumens, Phys. Rev. Lett. **84**, 5300 (2000).

[75] R. A. Wilhelm, E. Gruber, V. Smejkal, S. Facsko, and F. Aumayr, Phys. Rev. A **93**, 052708 (2016).